american physiological society
PHYSIOLOGICAL GENOMICS

Physiol Genomics 56: 661–671, 2024.
First published August 19, 2024; doi:10.1152/physiolgenomics.00057.2024

RESEARCH ARTICLE

Gill ionocyte remodeling mediates blood pH regulation in rockfish (*Sebastes diploproa*) exposed to environmentally relevant hypercapnia

Garfield T. Kwan, Alexander M. Clifford, Kaelan J. Prime, Till S. Harter, and Martin Tresguerres

Marine Biology Research Division, Scripps Institution of Oceanography, University of California, San Diego, California, United States

Abstract

Marine fishes excrete excess H^+ using basolateral Na^+-K^+-ATPase (NKA) and apical Na^+/H^+ exchanger 3 (NHE3) in gill ionocytes. However, the mechanisms that regulate H^+ excretion during exposure to environmentally relevant hypercapnia (ERH) remain poorly understood. Here, we explored transcriptomic, proteomic, and cellular responses in gills of juvenile splitnose rockfish (*Sebastes diploproa*) exposed to 3 days of ERH conditions (pH ~7.5, ~1,600 μatm P_{CO_2}). Blood pH was fully regulated at ~7.75 despite a lack of significant changes in gill *1*) mRNAs coding for proteins involved in blood acid-base regulation, *2*) total NKA and NHE3 protein abundance, and *3*) ionocyte density. However, ERH-exposed rockfish demonstrated increased NKA and NHE3 abundance on the ionocyte plasma membrane coupled with wider apical membranes and greater extension of apical microvilli. The observed gill ionocyte remodeling is consistent with enhanced H^+ excretion that maintains blood pH homeostasis during exposure to ERH and does not necessitate changes at the expression or translation levels. These mechanisms of phenotypic plasticity may allow fishes to regulate blood pH during environmentally relevant acid-base challenges and thus have important implications for both understanding how organisms respond to climate change and for selecting appropriate metrics to evaluate its impact on marine ecosystems.

NEW & NOTEWORTHY Splitnose rockfish exposed to environmentally relevant hypercapnia utilize existing proteins (rather than generate additional machinery) to maintain homeostasis.

acidosis; ocean acidification; slc9a3; transcriptomics; upwelling

INTRODUCTION

Many marine environments regularly experience elevated P_{CO_2} levels ("hypercapnia") of variable magnitude and duration. For instance, P_{CO_2} in kelp forests, coral reefs, and tide pools can easily reach up to 1,000 μatm (pH ~7.70) on a nightly basis due to the respiration of residing organisms [for a review, see Tresguerres et al. (1)]. Upwelling events can induce surges in P_{CO_2} that reach levels higher than 1,200 μatm (pH ~7.6) at the ocean surface for several days to weeks (2–7). On a longer timescale, anthropogenic ocean acidification (OA) is predicted to increase global average surface ocean P_{CO_2} levels to ~1,000 μatm P_{CO_2} by the year 2100 and to ~2,000 μatm P_{CO_2} (pH ~7.4) by the year 2300 (8).

Exposure to hypercapnia results in blood acidosis in aquatic animals. To avoid negative effects on gas transport and other physiological functions, marine fishes mitigate blood acidosis using specialized gill ion-transporting cells called "ionocytes." These cells express abundant basolateral Na^+-K^+-ATPase (NKA) that generates the driving force for excreting H^+ into seawater in exchange for Na^+ through apical Na^+/H^+ exchanger 3 (NHE3; slc9a3) (9). It is well established that marine fishes chronically exposed to severe hypercapnia (>6,000 μatm P_{CO_2}, pH < 7.00) increase the abundance of gill NKA and NHE3 mRNA and protein (10–12), which results in greater H^+ excretion from the blood into seawater to restore nominal blood pH levels (12, 13).

In contrast, the mechanisms that upregulate H^+ excretion during exposure to environmentally relevant hypercapnia (ERH) are less clear. Only a few studies have studied the gill ion-transporting mechanisms underlying blood pH regulation in marine fishes exposed to ERH. The Gulf toadfish (*Opsanus beta*) regulated blood pH during 3-day exposures to 1,900 μatm P_{CO_2} (14). Unlike the responses of marine fishes to chronic severe hypercapnia, toadfish gill NKA activity significantly decreased after 24 h of exposure to ERH and then reverted back to control levels by 72 h (14). Atlantic cod (*Gadus morhua*) upregulated the mRNA abundance of three gill NKA α-subunit isoforms after a 28-day exposure to 1,200 μatm P_{CO_2} (but not to more severe levels of 2,200 μatm P_{CO_2}); however, gill NKA protein abundance and activity remained unchanged (but blood pH was not measured) (15). Red drum (*Sciaenops ocellatus*) fully regulated blood pH after a 14-day exposure to 1,000 μatm P_{CO_2} and significantly increased gill NKA activity (16), and a follow-up study did not detect any changes in NHE3 mRNA abundance under comparable

Correspondence: G. T. Kwan (gkwan09@gmail.com); M. Tresguerres (mtresguerres@ucsd.edu).
Submitted 16 May 2024 / Revised 10 July 2024 / Accepted 8 August 2024

1094-8341/24 Copyright © 2024 the American Physiological Society.

Downloaded from journals.physiology.org/journal/physiolgenomics by Kathleen Pleet (073.135.252.129) on September 16, 2024.

conditions (17). European seabass (*Dicentrarchus labrax*) also regulated blood pH during exposure to 1,000 μatm P_{CO_2}, where gill NKA mRNA expression remained unchanged over the first 3 and 7 days but was upregulated after 21 days of hypercapnic exposure (although protein abundance was not measured) (18). Altogether, these studies indicate that marine fishes can fully regulate blood pH during ERH exposure. However, the experimental differences between studies, the variable and small changes in gill NKA and NHE3 abundances, and the disconnect between mRNA expression and protein abundance currently do not allow clear generalizations on the physiological mechanisms of plasticity that regulate blood pH during ERH.

More recently, it was reported that European seabass exposed to 10,000 μatm P_{CO_2} (pH ∼6.90) were able to regulate blood pH within 2 h (19). These fish did not experience any changes in gill NKA or NHE3 protein abundance; however, immunohistochemical observations revealed that the gill NKA-rich ionocytes had significantly increased apical surface area with NHE3 on them. These results indicated blood pH regulation was achieved via activation of preexisting gill NKA and NHE3 proteins. However, it is not clear whether this mechanism is specific to European seabass or whether it is relevant during longer exposures to EHR.

In addition to NKA and NHE3, V-type H^+-ATPase (VHA) has been proposed to excrete H^+ to compensate a blood acidosis in marine fishes, as is the case in freshwater fishes (20). Although VHA mRNA abundance was upregulated in some cases during exposure to ERH, there was little correlation between VHA mRNA expression and protein abundance (15, 17), and VHA was not observed in the apical membrane of gill cells (17), where it would be expected to be found should it play a role in H^+ excretion.

We recently reported that juvenile splitnose rockfish (*Sebastes diploproa*) have two types of gill ATPase-rich cells. One is the archetypical NKA-rich ionocyte, which additionally expresses VHA throughout its cytoplasm. The other one has abundant VHA in its basolateral membrane and does not express detectable NKA, and its function is still unclear (20). We also reported that these fish were able to fully regulate blood pH upon exposure to ERH (1,600 μatm P_{CO_2}, pH ∼7.5, for 3 days) and identified the physiological mechanism that links blood and endolymph acid-base regulation with otolith overgrowth (21). In the present study, we examined the gills from those same rockfish to investigate the molecular and cellular mechanisms underlying blood acid-base regulation in response to ERH. Specifically, we analyzed the following in splitnose rockfish gills: *1*) transcriptomic responses using RNA sequencing (RNA-seq); *2*) NKA, NHE3, and VHA protein abundance in crude homogenates and membrane-enriched fractions using Western blot analysis; *3*) NKA-rich ionocyte and VHA-rich cell abundance as well as NKA, NHE3, and VHA subcellular localization using immunohistochemistry and confocal microscopy; and *4*) NKA-rich ionocyte apical morphology using scanning electron microscopy. Our integrative physiological genomics approach indicated that the full compensation of rockfish blood pH during ERH involves a functional remodeling of gill ionocytes by translocating existing NKA and NHE3 proteins into the plasma membrane of ionocytes together with an extension of apical microvilli that collectively upregulated H^+ excretion into seawater.

METHODS

Experimental Animals, Tissues, and Setup

The gill samples analyzed in this study were dissected from the same splitnose rockfish reported in Kwan and Tresguerres (21). Rockfish were caught from drifting kelp paddies off the coast of La Jolla, CA, and raised in the Hubbs Experimental Aquarium at Scripps Institution of Oceanography at the University of California, San Diego (SIO-UCSD, La Jolla, CA; California Department of Fish and Wildlife Permit No. SCP13227). Rockfish average length and weight were 12.08 ± 0.18 cm and 45.54 ± 1.89 g (means ± SE, $N = 21$), respectively.

Briefly, two header tanks were supplied with ambient seawater: the control header tank was not manipulated, and its P_{CO_2} and pH were 571.90 ± 4.88 μatm and 7.89 ± 0.012, respectively, whereas the ERH header tank was bubbled with CO_2 using a pH-stat system (IKS Aquastar, Karlsbad, Germany) to adjust P_{CO_2} and pH to 1,591.56 ± 18.58 μatm and 7.49 ± 0.01, respectively. Header tank-supplied water flowed into 3-L experimental tanks (flow rate = 0.3 L/min) where rockfish were individually housed. After a 12-h acclimation period, fish were exposed to control or ERH treatment conditions for 72 h. Rockfish were not fed throughout the experiment to ensure similar metabolic states. The experiment was repeated three times, with three controls and three ERH-exposed rockfish. No mortality was observed.

Blood and gill sampling, blood pH and plasma total CO_2 measurements, and plasma P_{CO_2}, HCO_3^- concentration, and CO_3^{2-} concentration calculations were performed, as previously described by Kwan and Tresguerres (21). A blood aliquot was loaded in a capillary tube, centrifuged (500 *g*, 3 min), and used to determine hematocrit. After euthanasia, gill samples were dissected and fixed for immunohistochemistry (first right arch) or scanning electron microscopy (first left arch), immersed in RNAlater for RNA-seq analysis (second right arch), or flash frozen in liquid nitrogen for Western blot analysis (second left arch). All experiments were approved by the SIO-UCSD animal care committee under the Institutional Animal Care and Use Committee Protocol (No. S10320).

RNA Extraction, Sequencing, and Analysis

Gill samples were incubated in RNAlater for 24 h at 4°C and then stored at −20°C until processing. Frozen samples were then thawed on ice, blotted dry, transferred to a 2-mL tube containing TRIzol Reagent, and homogenized on ice with a handheld motorized mortar and pestle (Kimble/Kontes, Dusseldorf, Germany). The TRIzol homogenate was briefly centrifuged to pellet debris, and the supernatant was processed for RNA extraction (RNAEasy Mini, Qiagen) according to the manufacturer's specifications with an on-column DNAase I treatment to digest trace genomic DNA. RNA quantity and purity were determined via spectrophotometry (Nanodrop, Thermo Scientific). RNA integrity was determined using an Agilent 2100 Bioanalyzer (Agilent, Santa Clara, CA). High-quality RNA samples (RNA integrity number > 8) were used to construct individual poly-A enriched cDNA libraries by Novogene (Beijing, China) using the Illumina TruSeq RNA

Downloaded from journals.physiology.org/journal/physiolgenomics by Kathleen Pleet (073.135.252.129) on September 16, 2024.

Sample Preparation Kit (Illumina, San Diego, CA) according to the manufacturer's protocol. Briefly, mRNA was purified from total RNA using oligo(dt) magnetic beads, and the retained mRNA was chemically sheared into shorter fragments, followed by cDNA synthesis using random hexamer primers. The cDNA was fitted with Illumina adaptor primers and subjected to end-repair processing. After agarose gel electrophoresis, 200- to 300-bp fragments were extracted and used as templates for PCR amplification and cDNA library preparation. Libraries were sequenced using the Illumina NovoSeq 6000 platform to generate unstranded 150-bp paired-end reads (n = 6, Q30 > 83%). Raw sequencing reads were analyzed, trimmed of adaptor sequences, and processed to remove *1*) low-quality reads (qualified quality phred score < 20), *2*) reads containing >50% unqualified bases (base quality < 5), and *3*) reads possessing >10 unknown bases (Ns) with fastp (22). The remaining unpaired reads were discarded from downstream analysis. Standard RNA-seq quality control metrics are shown in Supplemental Table S1.

S. diploproa gill quality reads were aligned and mapped to the published genome of honeycomb rockfish (*S. umbrosus*; NCBI Accession No. PRJNA562005, fSebUmb1.pri, downloaded November 3, 2020) using HISAT2 (V2.1.0) (23). Mapped reads were assembled into transcripts and merged among samples, and this merged transcript file was used to quantify gene and transcript abundance in each sample using Stringtie (V2.1.2) 24, 25). Final gene and transcript quantitation data were analyzed with R using DESeq2 (26). Genes of low abundance (average abundance < 1 across all samples) and very low expression (summed counts < 5 across all samples) were filtered from the expression matrix. Following initial DESeq2, expression data were again normalized to remove differences across technical sources of variation using RUVseq (27), and data were processed again using DESeq2.

Antibodies

NKA was immunodetected using a mouse monoclonal antibody against the α-subunit of chicken NKA (a5, Developmental Studies Hybridoma Bank, Iowa City, IA) (28). NHE3 was immunodetected using custom-made rabbit antibodies against two epitope regions within rainbow trout (*Oncorhynchus mykiss*) NHE3b (GDEDFEFSEGDSASG and PSQRAQLRLPWTPSNLRRLAPL) (29). VHA was immunodetected using custom-made rabbit polyclonal or mouse monoclonal antibodies (GenScript) against a highly conserved epitope within VHA subunit B (AREEVPGRRGFPGY) (30, 31). These three primary antibodies were validated in splitnose rockfish (Supplemental Fig. S1) (21). The secondary antibodies were goat anti-mouse horseradish peroxidase linked and goat anti-rabbit horseradish peroxidase linked (Bio-Rad, Hercules, CA) for immunoblot analysis and goat anti-rabbit Alexa Fluor 488 and goat anti-mouse Alexa Fluor 568 (Invitrogen) for immunohistochemistry.

Western Blot Analysis

Frozen gill samples were immersed in liquid nitrogen, pulverized using a porcelain mortar and pestle, and submerged within ice-cold buffer containing protease inhibitors (250 mmol/L sucrose, 1 mmol/L EDTA, 30 mmol/L Tris, 10 mmol/L benzamidine hydrochloride hydrate, 1 mmol/L phenylmethanesulfonyl fluoride, and 1 mmol/L dithiothreitol, pH 7.5). Samples were centrifuged at 3,000 *g* (10 min, 4°C) to remove cell debris, and the resulting supernatant was saved as the "crude homogenate." A portion of the crude homogenate was further centrifuged at 21,130 *g* (30 min, 4°C), and the pellet was saved as the "membrane-enriched" fraction. Total protein concentration in both fractions was determined using the Bradford assay (32) and stored at −80°C if not used on the same day. On the day of SDS-electrophoresis, the samples were mixed with an equal volume of 2× Laemmli buffer containing 10% β-mercaptoethanol, heated (70°C for 5 min), and loaded (crude homogenate: 10 μg per lane; membrane: 2 μg per lane) onto a 7.5% polyacrylamide mini gel (Bio-Rad). Proteins in the samples were separated by polyacrylamide gel electrophoresis at 200 V for 40 min, and the separated proteins were transferred onto a polyvinylidene difluoride (PVDF) membrane using a wet transfer cell (Bio-Rad) at 100 mA (4°C overnight). On the following day, PVDF membranes were incubated in Tris-buffered saline with 1% Tween (TBS-T) with skim milk powder (0.1 g/mL) for 1 h and then incubated with primary antibody (NKA: 10.5 ng/mL, NHE3: 1:1,000, and VHA: 3 μg/mL in blocking buffer) at 4°C overnight. The next day, PVDF membranes were washed in TBS-T (3 × 10 min), incubated in blocking buffer with the appropriate secondary antibodies (1:10,000 in blocking buffer) for 1 h, and washed again in TBS-T (3 × 10 min). Bands were made visible through the addition of enhanced chemiluminescence Prime Western Blotting Detection Reagent (GE Healthcare, Waukesha, WI) and imaged and quantified in a Universal III Hood (Bio-Rad) using Image Lab software (version 6.0.1, Bio-Rad). Following imaging, the PVDF membrane was incubated in Ponceau stain (10 min, room temperature) to estimate protein loading. Relative NKA, NHE3, and VHA protein abundances were normalized to the protein content within each lane.

Immunohistochemistry

Rockfish gill samples were fixed in 4% paraformaldehyde in PBS (pH 7.4) on a shaker at 4°C overnight, immersed in 50% ethanol for 8 h, and stored in 70% ethanol at 4°C until processing. Fixed samples were rehydrated in PBS + 0.1% Tween (PBS-T) for 5 min, rinsed in ice-cold PBS containing 1.5 mg/mL $NaBH_4$ (6 × 10 min), and then incubated in blocking buffer (PBS-T, 2% normal goat serum, and 0.02% keyhole limpet hemocyanin) for 1 h at room temperature. Following this, samples were incubated with primary antibodies (NKA: 40 ng/mL, NHE3: 1:500, and VHA: 6 μg/mL in blocking buffer) at 4°C overnight. On the next day, samples were washed in PBS-T and incubated with blocking buffer containing secondary antibodies (1:500) and the nuclear dye DAPI (1 μg/mL) for 1 h at room temperature. The stained gill samples were then washed in PBS-T, whole mounted onto depressed glass slides fitted with a glass coverslip (No. 1.5, 0.17 mm), and imaged using a Zeiss inverted confocal microscope (AxioObserver Z1 with LSM800, Oberkochen, Germany) and Zeiss ZEN 2.6 blue edition software. To quantify gill NKA- and VHA-rich cell abundance, immunostained whole mounted gill samples were imaged using ×10 and ×20

Downloaded from journals.physiology.org/journal/physiolgenomics by Kathleen Pleet (073.135.252.129) on September 16, 2024.

objective lenses (EC Plan-Neofluar ×10/0.30 Ph 1 and Plan-Apochromat ×20/0.8 M27) and optimized settings for Alexa Fluor 488 (to visualize VHA, excitation 493 nm at 0.5% laser power, emission 517 nm, detection 510–575 nm), Alexa Fluor 568 (to visualize NKA, excitation 577 nm at 0.2% laser power, emission 603 nm, detection 575–617 nm), and DAPI (to visualize nuclei, excitation 353 nm at 0.2% laser power, emission 465 nm, detection 410–470 nm). *Z*-stacks were produced as the maximum intensity projection of ∼70 to 500 consecutive ∼1.93-µm optical sections. Average NKA- and VHA-rich ionocyte abundances were quantified in the proximal, medial, and distal sections of gill filaments (defined as in Ref. 29) (Fig. 1*A*) using the FIJI cell counter plugin (33). From each of nine control and nine ERH-exposed rockfish ($N = 9$), the numbers of NKA- and VHA-rich ionocytes were quantified after double-blind randomization in five lamellae from three filaments (total of 15 lamellae), which were averaged together for each replicate.

The subcellular localization of NKA, NHE3, and VHA was examined using ×40 and ×63 objective lenses (Zeiss LD LCI Plan-Apochromat ×40/1.2 lmm Korr DIC M27 and Plan-Apochromat ×63/1.40 Oil DIC M27) and optimized settings for Alexa Fluor 488 (to visualize VHA or NHE3, excitation 493 nm at 0.6–1.0% laser power, emission 517 nm, and detection 510–575 nm), Alexa Fluor 568 (to visualize NKA or NHE3, excitation 577 nm at 0.6–1.2% laser power, emission 603 nm, and detection 575–617 nm), and DAPI (to visualize nuclei, excitation 353 nm at 0.6–1.0% laser power, emission 465 nm, and detection 410–470 nm). *Z*-stacks of gill ionocytes were visualized as the maximum intensity projection of ∼70 to 250 consecutive ∼0.25-µm optical sections and analyzed using orthogonal cuts across the *X-Z* and *Y-Z* planes. Observations were conducted on five control and five ERH rockfish, on three filaments per rockfish.

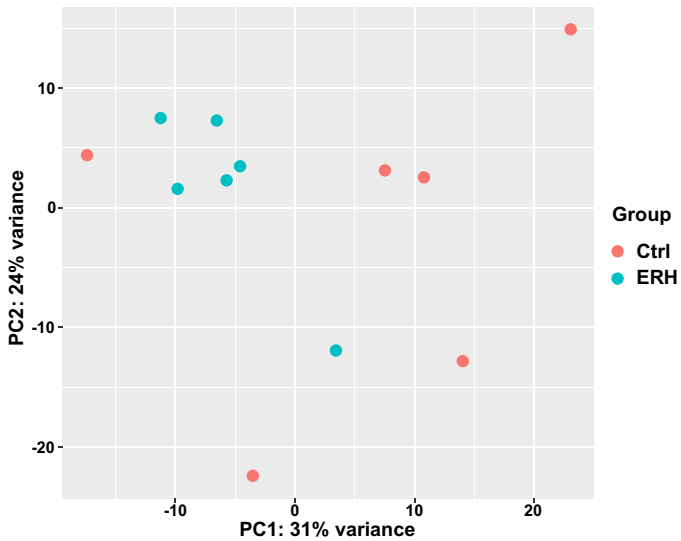


Figure 1. Principal component analysis of gene expression profiles. Gene expression was visualized by the first two principal components (PC1: 31% and PC2: 24%). Each point represents an individual fish, and colors denote exposure to control (Ctrl; ∼570 µatm CO_2, pH ∼7.9) or environmentally relevant hypercapnia (ERH; ∼1,600 µatm CO_2, pH ∼7.5) conditions ($N = 6$).

Scanning Electron Microscopy

Rockfish gill samples were fixed in 3% paraformaldehyde and 0.35% glutaraldehyde in 0.1 M cacodylate buffer overnight at 4°C and processed as previously described by Kwan et al. (34). Briefly, the samples were dehydrated in 50% ethanol for 8 h and stored in 70% ethanol. On the day of processing, fixed gill samples were dehydrated in 100% *tert*-butyl alcohol applying 25% increments over 24 h, frozen in 100% *tert*-butyl alcohol at 4°C, and freeze-dried using a VirTis benchtop freeze dryer (SP Industries, Gardiner, NY). Samples were then sputter coated with gold and imaged using a ThermoFisher Apreo 1 with Apreo LoVac field emission gun under low-vacuum mode (20 kV, 1.6 nA, and ∼0.03 mbar). Imaging was focused on the cells localized along the basal portion of the gill lamellae. The tasks of imaging, random assignment, and blind analysis of five ionocytes per rockfish ($N = 8$ control and $N = 9$ ERH) were performed by different investigators to ensure unbiased data collection.

Statistical Analysis

Statistical tests were performed using R [version 4.0.3, R Development Core Team (35)]. Normalized RNA-seq data were converted to the global Pearson's intersample correlational coefficient and analyzed as distance values to infer relative differences between libraries and to generate a hierarchical clustering profile using R and the MDS package. Principal component analysis (PCA) on the normalized data was conducted using DESeq2. Differentially expressed genes (DEGs; $\log_2$ fold change ≥ 2) were identified based on significance (α of 0.05). Gene Ontology (GO) and Kyoto Encyclopedia of Genes and Genomes (KEGG) enrichment analysis was performed using gProfiler (biit.cs.ut.ee/gprofiler) (36). Differences in the variance of each gene were assessed using Levene's test.

Protein abundance, hematocrit, and apical morphology datasets were analyzed with Student's *t* test (two-tailed). NKA- and VHA-rich ionocyte abundances were analyzed using two-way ANOVA with treatment and gill filament section as factors. Statistical assumptions of normality and homoscedasticity were assessed using the Shapiro-Wilk and *F* tests, respectively. Membrane-enriched NKA abundance required an inverse transformation, whereas membrane-enriched VHA abundance required a square root transformation to meet the parametric requirements. The scanning electron microscopy-based apical morphology dataset failed to meet the assumptions of normality even after transformation and was analyzed using the nonparametric Wilcoxon rank sum test (two-tailed) with continuity correction. An α of 0.05 was used for all datasets. Values are reported as means ± SE.

RESULTS

We have previously reported that rockfish exposed to ERH (∼1,600 µatm P_{CO_2}, pH ∼7.5) for 3 days completely regulated blood pH (ERH: 7.85 ± 0.04 and control: 7.75 ± 0.03) and that their blood plasma had significantly higher HCO_3^- concentration (ERH: 5.16 ± 0.31 mM and control: 2.37 ± 0.20 mM; 21). Here, we additionally reported a significant ∼15% increase in

Downloaded from journals.physiology.org/journal/physiolgenomics by Kathleen Pleet (073.135.252.129) on September 16, 2024.

hematocrit in ERH-exposed rockfish (30 ± 1.0% vs. 26 ± 1.3% in controls).

Maintenance of blood pH combined with plasma HCO_3^- accumulation indicated active and effective blood acid-base regulation in response to ERH. As a first step to elucidate the underlying mechanisms, we performed RNA-seq in gills from control and ERH-exposed rockfish. The RNA-seq data mapped to 24,577 genes annotated in the honeycomb rockfish genome, and PCA revealed two components that together accounted for 55% of the total variation in our dataset (PC1 = 31% and PC2 = 24%). The gene expression dispersal pattern in control rockfish was stochastic, whereas that in ERH-exposed rockfish was more tightly clustered together (Fig. 1).

However, only 94 genes (<0.4% of the total) were differentially expressed in ERH-exposed fish: 65 upregulated (Supplemental Table S2) and 29 downregulated (Supplemental Table S3). GO and KEGG analyses (false discovery rate ≤ 0.01) failed to identify differentially enriched pathways. An analysis of DEGs revealed strong upregulation of genes coding for transcription factors and splicing regulators (RNA-binding motif 20 and zinc finger protein 239), for proteins implicated in angiogenesis and vascularization (neuropeptide Y receptor y_2 and acetylcholine receptor subunit α_7), and for others involved in cell adhesion and cytoskeletal remodeling (contactin 3a, collagen, laminin-β, and calpain-5; Supplemental Tables S2 and S3). However, the mRNA

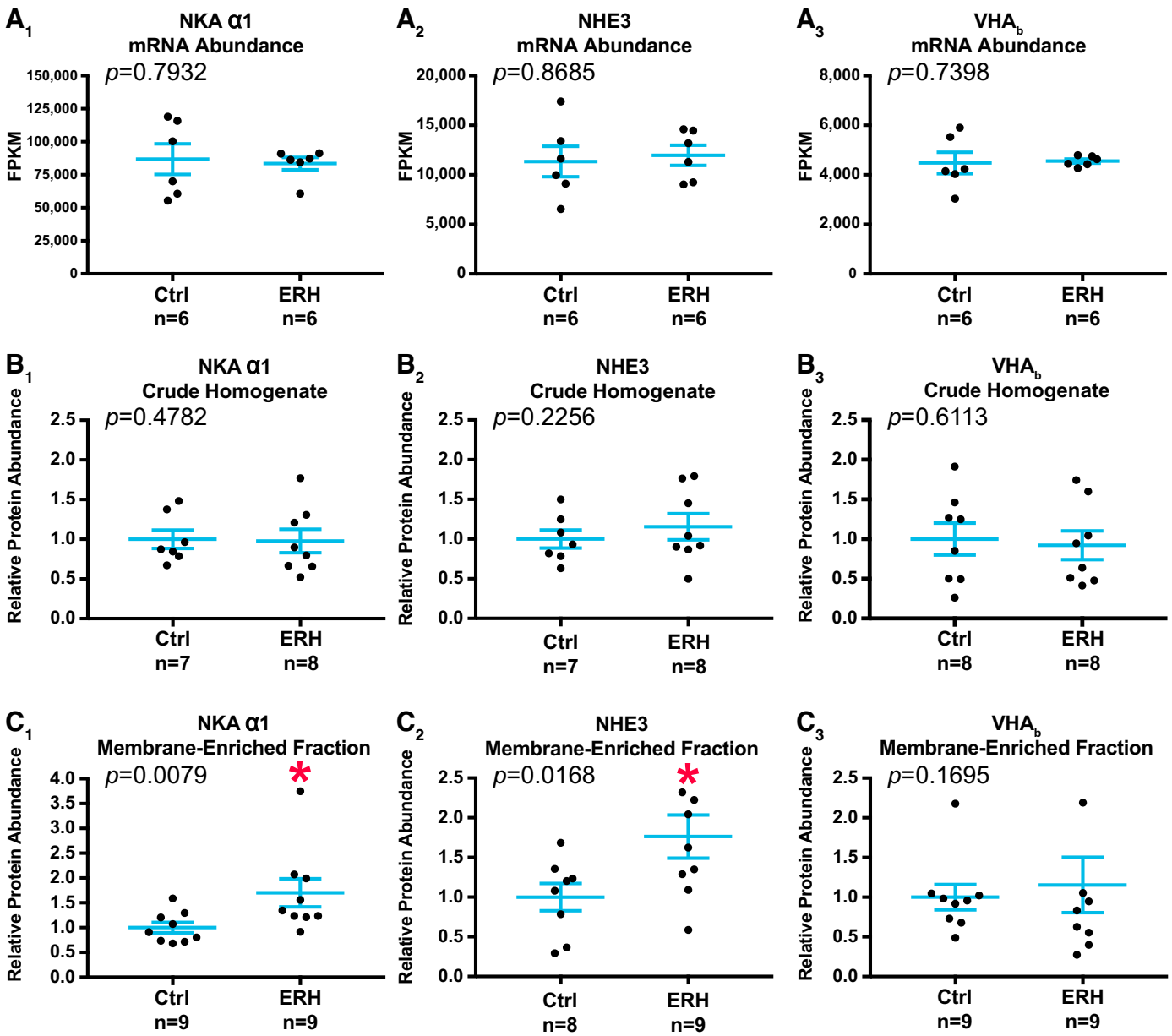


Figure 2. Gene expression and protein abundance in gills from control (Ctrl) rockfish and rockfish exposed to environmentally relevant hypercapnia (ERH). Ctrl fish were exposed to Ctrl conditions (~570 μatm CO_2, pH ~7.9); ERH fish were exposed to ERH conditions (~1,600 μatm CO_2, pH ~7.5). *A*–*C*: mRNA abundance (*A*), total protein abundance in the crude homogenate (indicative of total abundance; *B*), and protein abundance in the membrane-enriched fraction (*C*) of Na^+-K^+-ATPase α-subunit (NKA; *1*), Na^+/H^+ exchanger 3 (NHE3; *2*), and V-type H^+ ATPase subunit B (VHA_B; *3*). *Significant difference. Values are means ± SE. FPKM, fragments per kilobase of transcript per million mapped reads.

Downloaded from journals.physiology.org/journal/physiolgenomics by Kathleen Pleet (073.135.252.129) on September 16, 2024.

abundances of genes coding for proteins with established functions in fish acid-base and ion regulation were unchanged (Fig. 2, *A1–A3*, and Supplemental Fig. S2), suggesting that blood acid-base regulation during ERH did not involve a transcriptional response. Alternatively, changes in mRNA levels could have taken place in the early phase of ERH exposure, affecting the abundance of acid-base regulatory proteins, and returned to baseline levels by the time of sampling on *day 3*. We investigated this possibility by quantifying the protein abundances of NKA, NHE3, and VHA_B in rockfish gills.

The total abundances of NKA, NHE3, or VHA_B protein in rockfish gill homogenates (estimated Western blots in gill crude homogenates) did not differ between control and ERH-exposed rockfish (Fig. 2, *B1–B3*), indicating a lack of translational response. In contrast, the abundances of NKA and NHE3 protein in gill cell membrane-enriched fractions were 50% higher in ERH-exposed rockfish than in control rockfish (Fig. 2, *C1* and *C2*), whereas VHA_B protein abundance in gill cell membrane-enriched fraction remained unchanged (Fig. 2*C3*). These results suggested that ERH-exposed rockfish translocated preexisting NKA and NHE3 proteins into the plasma membrane of gill ionocytes to upregulate H^+ excretion to seawater and regulate blood pH.

Next, we used immunohistochemistry to examine whether exposure to ERH affected the abundance of NKA-rich ionocytes and VHA-rich cells in rockfish gills. As previously reported for most other fish species (37), NKA-rich ionocytes were much more abundant on the trailing edge than on the leading edge of rockfish gills (Fig. 3, *A–C*). Strikingly, however, the majority of these ionocytes were present along the bottom half of the gill lamellae (Fig. 3, *B* and *C*), which contrasts with most other fishes studied so far, which typically have ionocytes on the gill filament or at the base of the lamellae (29, 38). The abundance of VHA-rich cells was approximately half of that of NKA-rich ionocytes, and they were present on both

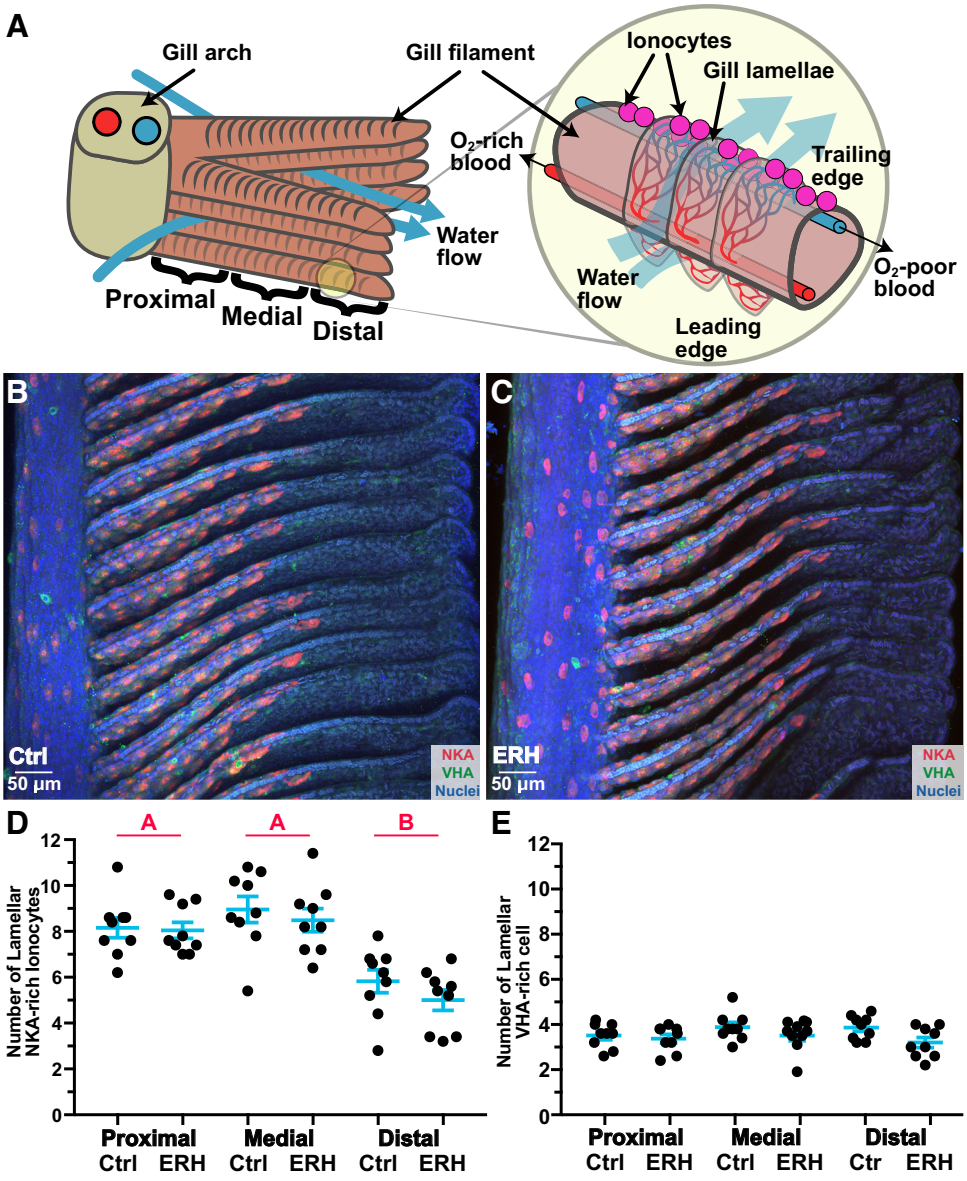


Figure 3. Na^+-K^+-ATPase (NKA)-rich ionocytes and V-type H^+-ATPase (VHA)-rich cells in gills from control (Ctrl) rockfish and rockfish exposed to environmentally relevant hypercapnia (ERH). *A*: diagram of a fish gill arch, filaments, and lamellae showing ionocytes in the trailing edge (pink circles). *B* and *C*: representative image of gills from Ctrl and ERH rockfish immunostained for NKA (red) and VHA (green). *D* and *E*: abundance of NKA-rich ionocytes and VHA-rich cells along the lamellae at the proximal, medial, and distal sections of gill filaments. $N = 9$. Values are means ± SE. ^{A,B}Significant difference in NKA-rich ionocyte abundance between filament sections; there were no significant differences between sections in VHA-rich cells or between control and ERH treatments in either cell type.

Downloaded from journals.physiology.org/journal/physiolgenomics by Kathleen Pleet (073.135.252.129) on September 16, 2024.

the leading and trailing edge of the filament as well as on the lamellae. A separate analysis along the proximal, medial, and distal portions of the gill filaments (see diagram in Fig. 3*A*) revealed that NKA-rich ionocytes were significantly more abundant on the proximal and medial sections than in the distal section, whereas VHA-rich cells did not differ among the sections. These patterns were unaffected by ERH exposure (Fig. 3, *D* and *E*, and Supplemental Table S4).

Higher magnification three-dimensional reconstructed confocal images of gill ionocytes revealed that NKA-rich ionocytes expressed NHE3 in the apical membrane (Fig. 4, *A* and *B*), NKA adjacent to the apical membrane but in the basolateral membrane tubular system (Fig. 4), and VHA in the cytoplasm (Fig. 4, *C* and *D*). Relative to control fish, ERH-exposed fish seemed to have a denser apical NHE3 signal and an NKA signal that extended toward the basal side of the ionocyte (Fig. 4*B*). These qualitative observations matched the Western blot results, and, together, they indicate insertion of NHE3 into the apical membrane and of NKA into the basolateral membrane of ionocytes. On the contrary, VHA-rich cells had VHA along the basolateral edge of the cell and did not express NKA or NHE3, and these patterns were unaffected by the ERH exposure (Supplemental Fig. S3).

Finally, we examined the apical morphology of rockfish gill ionocytes using scanning electron microscopy. In control fish, the majority of ionocytes had a smooth apical membrane surface (see example in Fig. 5*A*) and 15.0 ± 8.24% of the ionocytes that were randomly analyzed had extended apical microvilli (see example in Fig. 5*B*). Interestingly, ERH-exposed rockfish had 45.5 ± 10.54% of ionocytes with extended microvilli [or a significantly higher threefold increase ($P = 0.0253$); Fig. 5*C*].

DISCUSSION

After 3 days of exposure to ERH at 1,600 μatm P_{CO_2} (pH ~7.5), rockfish blood pH was maintained at 7.85 and their plasma HCO_3^- concentration more than doubled from ~2.4 to ~5.2 mM (21). These features are typical of active blood acid-base regulation upregulation in H^+ excretion to seawater and

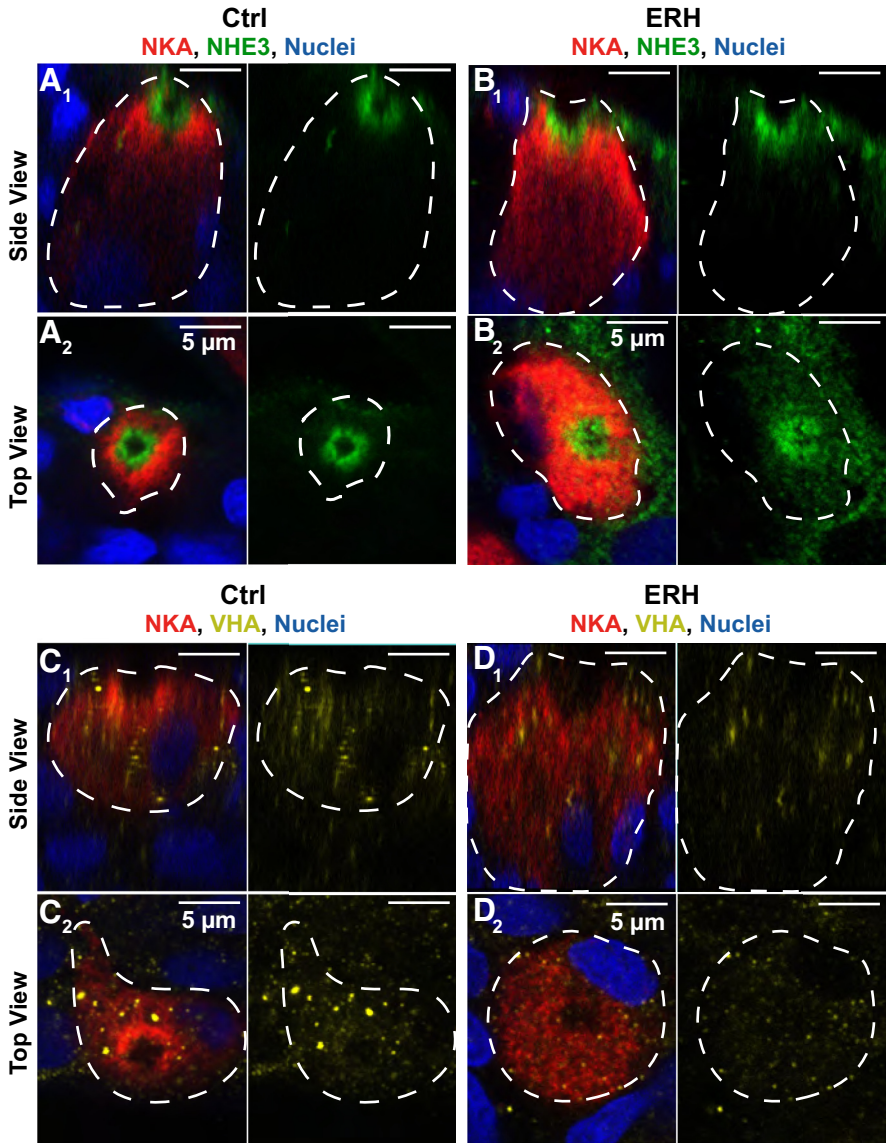


Figure 4. Protein localization in gill Na^+-K^+-ATPase (NKA)-rich ionocytes from control (Ctrl) rockfish and rockfish exposed to environmentally relevant hypercapnia (ERH). *A–D*: NKA, Na^+/H^+ exchanger 3 (NHE3), and V-type H^+ ATPase (VHA) expression within NKA-rich gill ionocytes after exposure to Ctrl (*A* and *B*) or ERH (*C* and *D*) conditions. Confocal images along the side view (*XZ* plane; *1*) and confocal images along the top view (*XY* plane; *2*) are shown. $N > 5$ per protein, per treatment. The white dashed lines indicate the boundaries of the NKA-rich ionocyte, which were determined with a transmitted photomultiplier (T-PMT). Scale bar = 5 μm. Lower magnification images are shown in Supplemental Fig. S4. Individual NKA and nucleus fluorescence images are shown in Supplemental Fig. S5.

Downloaded from journals.physiology.org/journal/physiolgenomics by Kathleen Pleet (073.135.252.129) on September 16, 2024.

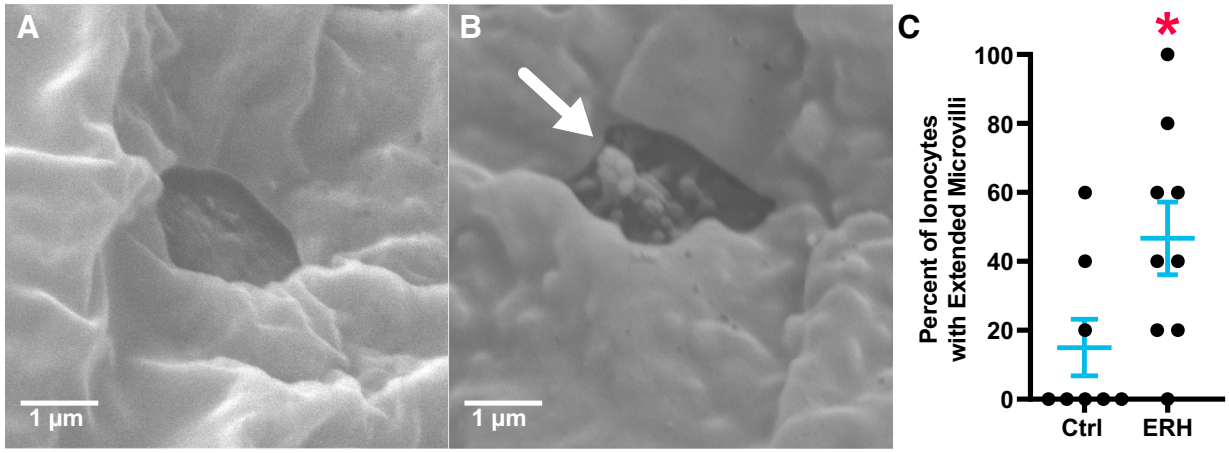


Figure 5. Apical morphology of gill ionocytes from control (Ctrl) rockfish and rockfish exposed to environmentally relevant hypercapnia (ERH). The apical surface of gill ionocytes could have retracted (*A*) or extended (*B*) microvilli (white arrow). *C*: blinded analysis of apical morphology revealed that rockfish exposed to ERH had significantly more ionocytes with extended microvilli than Ctrl fish. *Significant difference. Values are means ± SE; $N = 8$ Ctrl and $n = 9$ ERH.

in HCO_3^- absorption into the blood following activation of gill ion-transporting proteins. A priori, various mechanisms could fill this role, including *1*) upregulation of mRNA abundance leading to increased protein abundance of ion-transporting proteins; *2*) increased protein turnover (i.e., increased mRNA levels but constant protein levels); *3*) increased protein abundance independent of mRNA changes (translational response); *4*) posttranslational activation of preexisting proteins; or *5*) combinations of these mechanisms. In addition, the upregulation of H^+ excretion and HCO_3^- could have been related to a proliferation of gill ionocytes, which could confound the interpretation of the mRNA and protein quantification experiments. A systematic exploration ruled out all these options but the fourth one: the insertion of preexisting NKA and NHE3 into the basolateral and apical membranes of NKA-rich ionocytes coupled with microvilli extension to expand apical surface area (Fig. 6). Additional posttranslational modifications on NKA, NHE3, and other ion-transporting proteins, such as phosphorylation (39), are likely and deserve further examination.

The lack of significant changes in VHA mRNA, total protein, and membrane protein abundance; VHA-rich cell abundance; and VHA translocation to the apical membrane of any gill cell type all but rule out a role of gill VHA in excreting H^+ to seawater to compensate an ERH-induced blood acidosis. The roles of VHA in the gills of marine teleosts remain unknown. In NKA-rich ionocytes, it is unclear whether VHA is present in vesicles, in the basolateral membrane tubular system, or both. Although it is possible that VHA absorbs H^+ into the blood to compensate a postprandial blood alkalosis as shown in elasmobranchs (40, 41), it is not known if rockfish even experience a postprandial alkalosis. Alternatively, the observed VHA localization might correspond to lysosomes and play a role in digesting biological polymers for energy metabolism and cell structural maintenance. In VHA-rich cells, VHA is localized at the basolateral edge; however, the goblet shape of these cells and their ubiquitous presence throughout the gill epithelium resemble the mucus cells described in fish skin (42) and gills (43, 44) and may suggest a role in mucus production rather than in ion transport.

In addition to the gill responses, we found that ERH-exposed rockfish had a significant ~15% increase in hematocrit compared with controls, which resembles a previous report for European sea bass after acute exposure to pronounced hypercapnia (10,000 µatm P_{CO_2}, pH ~6.90 for 2 h) (19). Potential sources of this increased hematocrit are unknown but include erythropoiesis, adrenergic spleen contraction that releases red blood cells into the systemic circulation. Likewise, the effect of this increased hematocrit on blood gas transport capacity, acid-base regulation, and cardiac output remains to be determined.

The gill mRNA expression profile remained remarkably stable in the ERH-exposed rockfish, as only 94 of 24,577 genes (<0.4%) were differentially expressed and no GO or KEGG pathways were differentially enriched. Noteworthy, rockfish exposed to ERH for 72 h exhibited no significant changes in mRNA abundance of any genes coding for acid-base regulatory proteins. However, the distinct PCA clustering of gill samples from ERH-exposed rockfish indicates a more homogenous general transcriptomic profile compared with that of controls. Although we cannot pinpoint the underlying reasons, these patterns match the idea that gene expression is naturally stochastic and that a high variability in the basal general gene expression pattern can confer better adaptability in response to changing conditions (45). With this in mind, the more pronounced PCA clustering in ERH-fish may suggest a gene expression response to tune their physiology to the ERH. For example, the upregulation of many genes involved in angiogenesis and vascularization hints to links with the significantly higher Hct of ERH-exposed rockfish and perhaps also with their increased plasma HCO_3^- concentration. However, these highly speculative possibilities must be followed up with protein quantification and functional experiments to establish the potential significance of gene upregulation on rockfish physiology and their responses to ERH.

A synthesis of studies of marine fishes reveals a multi-tier gill ionocyte response to regulate blood pH in response to hypercapnia of increasing magnitude and duration (Fig. 6). The core acid-excreting mechanism in the gill ionocytes of

Downloaded from journals.physiology.org/journal/physiolgenomics by Kathleen Pleet (073.135.252.129) on September 16, 2024.

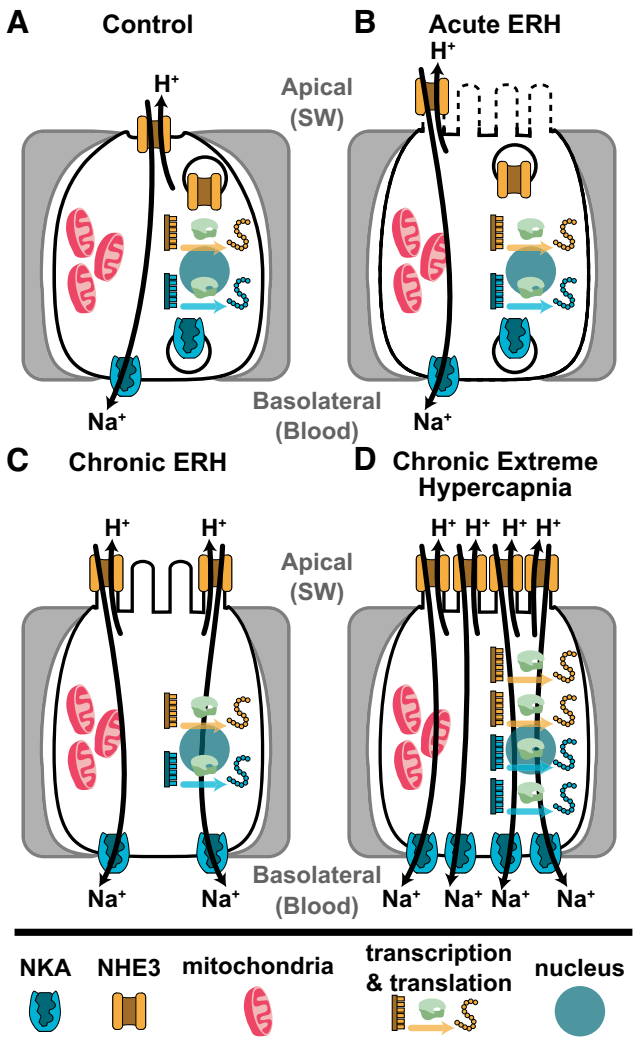


Figure 6. Putative mechanisms by which marine fish gill ionocytes regulate blood acid-base in response to hypercapnic challenges of different magnitudes and duration. *A*: under control (Ctrl) conditions, ionocytes have a baseline rate of H^+ excretion driven by basolateral Na^+-K^+-ATPase (NKA) and apical Na^+/H^+-exchanger 3 (NHE3); there are reserve pools of both transporters in the cytoplasm (potentially in vesicles) and gene transcription and translation are at baseline levels. *B*: during an acute environmentally relevant hypercapnia (ERH), H^+ excretion is upregulated via a widening of the ionocyte apical membrane. Other posttranslational regulatory mechanisms, such as microvilli extension (dotted lines) and phosphorylation, are likely. *C*: during a chronic ERH, H^+ excretion is further upregulated via insertion of the reserve pools of NKA and NHE3 into the basolateral and apical membranes, respectively, and by apical microvilli extension. *D*: during a chronic extreme hypercapnia, H^+ excretion is upregulated even further by increased transcription and translation of NKA and NHE3 (and possibly also other acid-base relevant proteins such as carbonic anhydrases and Na^+/HCO_3^- cotransporters). The additional NKA and NHE3 readily insert into the ionocyte plasma membrane.

marine fishes is based on basolateral NKA and apical NHE3. A pool of each of these transporters is constitutively membrane located and actively excreting H^+ that is produced by routine metabolism, whereas other pools are "on reserve" (Fig. 6*A*). The acute response to hypercapnia involves an increase of the NHE3-containing apical surface area (Fig. 6*B*) (19). This response is likely to be involved in the compensation of blood acidosis resulting from burst swimming, thus explaining why highly active fishes tend to be able to regulate blood pH in response to hypercapnia at a faster rate than more sluggish species (1, 19, 46). The chronic acid-base regulatory response depends on the magnitude of the hypercapnia.

During an ERH, fish additionally insert the reserve pools of NKA and NHE3 into ionocyte basolateral and apical membranes, respectively, and extend their apical microvilli to increase the surface area for NHE3-dependent H^+ excretion (Figs. 4, 5, and 6*C*). Like the acute response, the chronic response to ERH does not require the upregulation of ion-transporting proteins (Fig. 2) (14, 15, 17, 18). In contrast, the chronic response to severe hypercapnia (>6,000 μatm P_{CO_2}, pH < 7.00) additionally requires increased transcription and translation of NKA and NHE3 (Fig. 6*D*) (10–12). In all these cases, upregulation of H^+ excretion via the NKA-NHE3 machinery in gill ionocytes allows fishes to fully regulate their blood pH and compensate for the initial acidosis. However, H^+ excretion to seawater is accompanied by proportional absorption of HCO_3^- into plasma, and HCO_3^- accumulation in fish plasma has been linked to otolith overgrowth (21), increased skeletal biomineralization (47), neurobehavioral disturbances [Tresguerres and Hamilton (48)], and protection of cardiac function (49). In addition, HCO_3^- plays many important roles in mammalian physiology (50), which further highlights the need to study the effects of increased HCO_3^- concentration resulting from compensation of hypercapnia-induced blood acidosis on fishes. Another important consideration is that while ERH at nighttime in highly populated areas and during upwelling is associated with hypoxia, hypercapnia due to anthropogenic OA is not. This highlights the need for future experiments examining the interactions between environmental O_2 and CO_2/pH levels on the acid-base regulatory and metabolic responses of aquatic animals.

Conclusions

The use of RNA-seq, Western blot analysis on crude homogenates and membrane-enriched fractions, immunolocalization, scanning electron microscopy, and measurements of blood acid-base parameters allowed us to identify that rockfish exposed to an ERH regulate their blood pH by recruiting preexisting NKA and NHE3 into the basolateral and apical membranes of gill ionocytes, respectively. In contrast, no significant changes in gene or protein expression were involved. This integrative physiological genomic approach exemplifies the need to explore physiological responses to ERH (and, more broadly, to changing environments) at multiple levels of biological organization spanning from gene expression, protein abundance, intracellular localization, and whole animal physiology. In addition, our study highlights that homeostatic responses are tuned to the magnitude of the environmental or metabolic changes and that such tuning can be tracked down to the cellular level. These considerations are particularly important when studying the effects of OA on fish, as the underlying acid-base disturbance is relatively minor, and the associated compensatory responses may not be readily detectable using standard techniques.

DATA AVAILABILITY

Data will be made available upon reasonable request.

Downloaded from journals.physiology.org/journal/physiolgenomics by Kathleen Pleet (073.135.252.129) on September 16, 2024.

SUPPLEMENTAL MATERIAL

Supplemental Figs. S1–S5 and Supplemental Tables S1–S4: https://doi.org/10.6084/m9.figshare.26195576.v1.

GRANTS

This work was supported by National Science Foundation (NSF) Grant IOS 1754994 (to M.T.) as well as by NSF Graduate Research Fellowship and NSF Postdoctoral Research Fellowship in Biology (Award 1907334, to G.T.K.). We thank Phil Zerofski (SIO) for collecting the fish and helping with aquarium matters. We are grateful to Taylor Smith, Shane Finnerty, and Gabriel Lopez for the help with aquarium maintenance and fish care. The authors also thank Dr. Junya Hiroi (St. Marianna University School of Medicine, Kawasaki, Japan) for generously donating the anti-NHE3 antibodies and Sabine Faulhaber (University of California, San Diego) for technical assistance with the scanning electron microscope.

DISCLOSURES

No conflicts of interest, financial or otherwise, are declared by the authors.

AUTHOR CONTRIBUTIONS

G.T.K. and M.T. conceived and designed research; G.T.K., K.J.P., and T.S.H. performed experiments; G.T.K., A.M.C., K.J.P., T.S.H., and M.T. analyzed data; G.T.K., A.M.C., K.J.P., T.S.H., and M.T. interpreted results of experiments; G.T.K. and A.M.C. prepared figures; G.T.K. and M.T. drafted manuscript; G.T.K., A.M.C., K.J.P., T.S.H., and M.T. edited and revised manuscript; G.T.K., A.M.C., K.J.P., T.S.H., and M.T. approved final version of manuscript.

REFERENCES

1. **Tresguerres M**, **Clifford AM**, **Harter TS**, **Roa JN**, **Thies AB**, **Yee DP**, **Brauner CJ.** Evolutionary links between intra- and extracellular acid–base regulation in fish and other aquatic animals. *J Exp Zool A Ecol Integr Physiol* 333: 449–465, 2020 [Erratum in J Exp Zool A Ecol Integr Physiol. 333: 607, 2020]. doi:10.1002/jez.2367.
2. **Hofmann GE**, **Smith JE**, **Johnson KS**, **Send U**, **Levin LA**, **Micheli F**, **Paytan A**, **Price NN**, **Peterson B**, **Takeshita Y**, **Matson PG**, **Crook ED**, **Kroeker KJ**, **Gambi MC**, **Rivest EB**, **Frieder CA**, **Yu PC**, **Martz TR.** High-frequency dynamics of ocean pH: a multi-ecosystem comparison. *PLoS One* 6: e28983, 2011. doi:10.1371/journal.pone.0028983.
3. **Frieder CA**, **Nam SH**, **Martz TR**, **Levin LA.** High temporal and spatial variability of dissolved oxygen and pH in a nearshore California kelp forest. *Biogeosciences* 9: 3917–3930, 2012. doi:10.5194/bg-9-3917-2012.
4. **Kroeker KJ**, **Donham EM**, **Vylet K**, **Warren JK**, **Cheresh J**, **Fiechter J**, **Freiwald J**, **Takeshita Y.** Exposure to extremes in multiple global change drivers: characterizing pH, dissolved oxygen, and temperature variability in a dynamic, upwelling dominated ecosystem. *Limnol Oceanogr* 68: 1611–1623, 2023. doi:10.1002/lno.12371.
5. **Chavez FP**, **Sevadjian J**, **Wahl C**, **Friederich J**, **Friederich GE.** Measurements of pCO_2 and pH from an autonomous surface vehicle in a coastal upwelling system. *Deep Res Part II Top Stud Oceanogr* 151: 137–146, 2018. doi:10.1016/j.dsr2.2017.01.001.
6. **Takeshita Y**, **Frieder CA**, **Martz TR**, **Ballard JR**, **Feely RA**, **Kram S**, **Nam S**, **Navarro MO**, **Price NN**, **Smith JE.** Including high-frequency variability in coastal ocean acidification projections. *Biogeosciences* 12: 5853–5870, 2015. doi:10.5194/bg-12-5853-2015.
7. **Hamilton SL**, **Logan CA**, **Fennie HW**, **Sogard SM**, **Barry JP**, **Makukhov AD**, **Tobosa LR**, **Boyer K**, **Lovera CF**, **Bernardi G.** Species-specific responses of juvenile rockfish to elevated pCO_2: from behavior to genomics. *PLoS One* 12: e0169670, 2017. doi:10.1371/journal.pone.0169670.
8. **Goodwin P**, **Brown S**, **Haigh ID**, **Nicholls RJ**, **Matter JM.** Adjusting mitigation pathways to stabilize climate at 1.5°C and 2.0°C rise in global temperatures to year 2300. *Earth's Futur* 6: 601–615, 2018. doi:10.1002/2017EF000732.
9. **Hiroi J**, **McCormick SD.** New insights into gill ionocyte and ion transporter function in euryhaline and diadromous fish. *Respir Physiol Neurobiol* 184: 257–268, 2012. doi:10.1016/j.resp.2012.07.019.
10. **Deigweiher K**, **Koschnick N**, **Pörtner HO**, **Lucassen M.** Acclimation of ion regulatory capacities in gills of marine fish under environmental hypercapnia. *Am J Physiol Regul Integr Comp Physiol* 295: R1660–R1670, 2008. doi:10.1152/ajpregu.90403.2008.
11. **Melzner F**, **Göbel S**, **Langenbuch M**, **Gutowska MA**, **Pörtner HO**, **Lucassen M.** Swimming performance in Atlantic Cod (*Gadus morhua*) following long-term (4-12 months) acclimation to elevated seawater P(CO2). *Aquat Toxicol* 92: 30–37, 2009. doi:10.1016/j.aquatox.2008.12.011.
12. **Edwards SL**, **Wall BP**, **Morrison-Shetlar A**, **Sligh S**, **Weakley JC**, **Claiborne JB.** The effect of environmental hypercapnia and salinity on the expression of NHE-like isoforms in the gills of a euryhaline fish (*Fundulus heteroclitus*). *J Exp Zool A Comp Exp Biol* 303: 464–475, 2005. doi:10.1002/jez.a.175.
13. **Liu ST**, **Horng JL**, **Chen PY**, **Hwang PP**, **Lin LY.** Salt secretion is linked to acid-base regulation of ionocytes in seawater-acclimated medaka: new insights into the salt-secreting mechanism. *Sci Rep* 6: 31433, 2016. doi:10.1038/srep31433.
14. **Esbaugh AJ**, **Heuer R**, **Grosell M.** Impacts of ocean acidification on respiratory gas exchange and acid-base balance in a marine teleost, *Opsanus beta*. *J Comp Physiol B* 182: 921–934, 2012. doi:10.1007/s00360-012-0668-5.
15. **Michael K**, **Kreiss CM**, **Hu MY**, **Koschnick N**, **Bickmeyer U**, **Dupont S**, **Pörtner HO**, **Lucassen M.** Adjustments of molecular key components of branchial ion and pH regulation in Atlantic cod (*Gadus morhua*) in response to ocean acidification and warming. *Comp Biochem Physiol B Biochem Mol Biol* 193: 33–46, 2016. doi:10.1016/j.cbpb.2015.12.006.
16. **Esbaugh AJ**, **Ern R**, **Nordi WM**, **Johnson AS.** Respiratory plasticity is insufficient to alleviate blood acid-base disturbances after acclimation to ocean acidification in the estuarine red drum, *Sciaenops ocellatus*. *J Comp Physiol B*186: 97–109, 2016. doi:10.1007/s00360-015-0940-6.
17. **Allmon EB**, **Esbaugh AJ.** Carbon dioxide induced plasticity of branchial acid-base pathways in an estuarine teleost. *Sci Rep* 7: 45680, 2017. doi:10.1038/srep45680.
18. **Shrivastava J**, **Ndugwa M**, **Caneos W**, **De Boeck G.** Physiological trade-offs, acid-base balance and ion-osmoregulatory plasticity in European sea bass (*Dicentrarchus labrax*) juveniles under complex scenarios of salinity variation, ocean acidification and high ammonia challenge. *Aquat Toxicol* 212: 54–69, 2019. doi:10.1016/j.aquatox.2019.04.024.
19. **Montgomery DW**, **Kwan GT**, **Davison WG**, **Finlay J**, **Berry A**, **Simpson SD**, **Engelhard GH**, **Birchenough SNR**, **Tresguerres M**, **Wilson RW.** Rapid blood acid-base regulation by European sea bass (*Dicentrarchus labrax*) in response to sudden exposure to high environmental CO_2. *J Exp Biol* 225: jeb242735, 2022. doi:10.1242/jeb.242735.
20. **Tresguerres M**, **Kwan GT**, **Weinrauch A.** Evolving views of ionic, osmotic and acid–base regulation in aquatic animals. *J Exp Biol* 226: jeb245747, 2023. doi:10.1242/jeb.245747.
21. **Kwan GT**, **Tresguerres M.** Elucidating the acid-base mechanisms underlying otolith overgrowth in fish exposed to ocean acidification. *Sci Total Environ* 823: 153690, 2022. doi:10.1016/j.scitotenv.2022.153690.
22. **Chen S**, **Zhou Y**, **Chen Y**, **Gu J.** fastp: an ultra-fast all-in-one FASTQ preprocessor. *Bioinformatics* 34: i884–i890, 2018. doi:10.1093/bioinformatics/bty560.
23. **Kim D**, **Langmead B**, **Salzberg SL.** HISAT: a fast spliced aligner with low memory requirements. *Nat Methods* 12: 357–360, 2015. doi:10.1038/nmeth.3317.
24. **Kovaka S**, **Zimin AV**, **Pertea GM**, **Razaghi R**, **Salzberg SL**, **Pertea M.** Transcriptome assembly from long-read RNA-seq alignments with StringTie2. *Genome Biol* 20: 278, 2019. doi:10.1186/s13059-019-1910-1.
25. **Pertea M**, **Pertea GM**, **Antonescu CM**, **Chang TC**, **Mendell JT**, **Salzberg SL.** StringTie enables improved reconstruction of a

Downloaded from journals.physiology.org/journal/physiolgenomics by Kathleen Pleet (073.135.252.129) on September 16, 2024.

transcriptome from RNA-seq reads. *Nat Biotechnol* 33: 290–295, 2015. doi:10.1038/nbt.3122.
26. **Love MI**, **Huber W**, **Anders S.** Moderated estimation of fold change and dispersion for RNA-seq data with DESeq2. *Genome Biol* 15: 550, 2014. doi:10.1186/s13059-014-0550-8.
27. **Risso D**, **Ngai J**, **Speed TP**, **Dudoit S.** Normalization of RNA-seq data using factor analysis of control genes or samples. *Nat Biotechnol* 32: 896–902, 2014. doi:10.1038/nbt.2931.
28. **Lebovitz RM**, **Takeyasu K**, **Fambrough DM.** Molecular characterization and expression of the ($Na^+ + K^+$)-ATPase alpha-subunit in *Drosophila melanogaster*. *EMBO J* 8: 193–202, 1989. doi:10.1002/j.1460-2075.1989.tb03364.x.
29. **Christensen AK**, **Hiroi J**, **Schultz ET**, **McCormick SD.** Branchial ionocyte organization and ion-transport protein expression in juvenile alewives acclimated to freshwater or seawater. *J Exp Biol* 215: 642–652, 2012. doi:10.1242/jeb.063057.
30. **Kwan GT**, **Smith TR**, **Tresguerres M.** Immunological characterization of two types of ionocytes in the inner ear epithelium of Pacific Chub Mackerel (*Scomber japonicus*). *J Comp Physiol B* 190: 419–431, 2020. doi:10.1007/s00360-020-01276-3.
31. **Yee DP**, **Hildebrand M**, **Tresguerres M.** Dynamic subcellular translocation of V-type H^+ -ATPase is essential for biomineralization of the diatom silica cell wall. *New Phytol* 225: 2411–2422, 2020. doi:10.1111/nph.16329.
32. **Bradford MM.** A rapid and sensitive method for the quantitation of microgram quantities of protein utilizing the principle of protein-dye binding. *Anal Biochem* 72: 248–254, 1976. doi:10.1006/abio.1976.9999.
33. **Schindelin J**, **Arganda-Carreras I**, **Frise E**, **Kaynig V**, **Longair M**, **Pietzsch T**, **Preibisch S**, **Rueden C**, **Saalfeld S**, **Schmid B**, **Tinevez JY**, **White DJ**, **Hartenstein V**, **Eliceiri K**, **Tomancak P**, **Cardona A.** Fiji: an open-source platform for biological-image analysis. *Nat Methods* 9: 676–682, 2012. doi:10.1038/nmeth.2019.
34. **Kwan GT**, **Wexler JB**, **Wegner NC**, **Tresguerres M.** Ontogenetic changes in cutaneous and branchial ionocytes and morphology in yellowfin tuna (*Thunnus albacares*) larvae. *J Comp Physiol B Biochem B* 189: 81–95, 2019. doi:10.1007/s00360-018-1187-9.
35. **R Development Core Team.** *R: a Language and Environment for Statistical Computing*. Vienna, Austria: R Foundation for Statistical Computing, 2013. http://www.r-project.org
36. **Raudvere U**, **Kolberg L**, **Kuzmin I**, **Arak T**, **Adler P**, **Peterson H**, **Vilo J.** g:Profiler: a web server for functional enrichment analysis and conversions of gene lists (2019 update). *Nucleic Acids Res* 47: W191–W198, 2019. doi:10.1093/nar/gkz369.
37. **Evans DH**, **Piermarini PM**, **Choe KP.** The multifunctional fish gill: dominant site of gas exchange, osmoregulation, acid-base regulation, and excretion of nitrogenous waste. *Physiol Rev* 85: 97–177, 2005. doi:10.1152/physrev.00050.2003.
38. **Skelton ZR**, **McCormick LR**, **Kwan GT**, **Lonthair J**, **Neira C**, **Clements SM**, **Martz TR**, **Bresnahan PJ**, **Send U**, **Giddings SN**, **Sevadjian JC**, **Jaeger S**, **Feit A**, **Frable BW**, **Zerofski PJ**, **Torres M**, **Crooks JA**, **McCullough J**, **Carter ML**, **Ternon E**, **Miller LP**, **Kalbach GM**, **Wheeler DC**, **Ed Parnell P**, **Swiney KM**, **Seibert G**, **Minich JJ**, **Hyde JR**, **Hastings PA**, **Smith JE**, **Komoroske LM**, **Tresguerres M**, **Levin LA**, **Wegner NC.** Organismal responses to deteriorating water quality during the historic 2020 red tide off Southern California. *Elem Sci Anth* 12: 00067, 2024. doi:10.1525/elementa.2023.00067.
39. **Tresguerres M**, **Milsom WK**, **Perry SF.** CO_2 and acid-base sensing. In: *Carbon Dioxide*. San Diego, CA: Elsevier, 2019, p. 33–68.
40. **Roa JN**, **Munévar CL**, **Tresguerres M.** Feeding induces translocation of vacuolar proton ATPase and pendrin to the membrane of leopard shark (*Triakis semifasciata*) mitochondrion-rich gill cells. *Comp Biochem Physiol A Mol Integr Physiol* 174: 29–37, 2014. doi:10.1016/j.cbpa.2014.04.003.
41. **Tresguerres M**, **Katoh F**, **Fenton H**, **Jasinska E**, **Goss GG.** Regulation of branchial V-H^+-ATPase, Na^+/K^+-ATPase and NHE2 in response to acid and base infusions in the Pacific spiny dogfish (*Squalus acanthias*). *J Exp Biol* 208: 345–354, 2005. doi:10.1242/jeb.01382.
42. **Ottesen OH**, **Olafsen JA.** Ontogenetic development and composition of the mucous cells and the occurrence of saccular cells in the epidermis of Atlantic halibut. *J Fish Biol* 50: 620–633, 1997. doi:10.1111/j.1095-8649.1997.tb01954.x.
43. **Mir IH**, **Channa A.** Mucous cells in the gills of snow trout, *Schizothorax curvifrons* Heckel (Pisces, Cypriniformes, Cyprinidae). *Cytologia* 76: 213–218, 2011. doi:10.1508/cytologia.76.213.
44. **Alkan Z**, **Oğuz AR.** Investigation of gill mucus cells of Lake Van fish (*Alburnus tarichi*) during reproductive migration. *Fish Physiol Biochem* 47: 409–419, 2021. doi:10.1007/s10695-020-00921-6.
45. **de Jong TV**, **Moshkin YM**, **Guryev V.** Gene expression variability: the other dimension in transcriptome analysis. *Physiol Genomics* 51: 145–158, 2019. doi:10.1152/physiolgenomics.00128.2018.
46. **Melzner F**, **Gutowska M**, **Langenbuch M**, **Dupont S**, **Lucassen M**, **Thorndyke MC**, **Bleich M**, **Pörtner HO.** Physiological basis for high CO_2 tolerance in marine ectothermic animals: pre-adaptation through lifestyle and ontogeny? *Biogeosciences Discuss* 6: 4693–4738, 2009. doi:10.5194/bgd-6-4693-2009.
47. **Di Santo V.** Ocean acidification and warming affect skeletal mineralization in a marine fish. *Proc Biol Sci* 286: 20182187, 2019. doi:10.1098/rspb.2018.2187.
48. **Tresguerres M**, **Hamilton T.** Acid-base physiology, neurobiology and behaviour in relation to CO_2-induced ocean acidification. *J Exp Biol* 220: 2136–2148, 2017. doi:10.1242/jeb.144113.
49. **Lo M**, **Shahriari A**, **Roa JN**, **Tresguerres M**, **Farrell AP.** Differential effects of bicarbonate on severe hypoxia- and hypercapnia-induced cardiac malfunctions in diverse fish species. *J Comp Physiol B* 191: 113–125, 2021. doi:10.1007/s00360-020-01324-y.
50. **Cordat E**, **Casey JR.** Bicarbonate transport in cell physiology and disease. *Biochem J* 417: 423–439, 2009. doi:10.1042/BJ20081634.

Downloaded from journals.physiology.org/journal/physiolgenomics by Kathleen Pleet (073.135.252.129) on September 16, 2024.